

## Characterization of hot deformability of C-Mn-Si structural steels

Marek Opiela<sup>1\*</sup> , Mateusz Rakszawa<sup>1</sup>, Barbara Grzegorzczuk<sup>1</sup> , Jacek Trzaska<sup>1</sup> 

<sup>1</sup> Faculty of Mechanical Engineering, Department of Engineering Materials and Biomaterials, Silesian University of Technology, Konarskiego Street 18A, 44-100 Gliwice, Poland

\* Corresponding author e-mail: marek.opiela@polsl.pl

### ABSTRACT

The paper presents the evaluation of hot deformability of two types of structural steel grades, (0.25C-1Mn-0.25Si-CrNiMo and 0.75C-1Mn-0.25Si), in the process of continuous and intermittent compression of samples. Tests were conducted in Gleeble 3800 thermo-mechanical simulator, on axisymmetric specimens with diameter of 10 mm and the length of 12 mm. Continuous compression tests were performed in the temperature range from 900 to 1100 °C, at a rate of 0.3 s<sup>-1</sup> and 3 s<sup>-1</sup>, while intermittent tests, consisting of four-stage plastic deformation – simulating successive rolling passes, were done in the temperature range from 850 to 1000 °C, applying the same rates. Conducted research allowed determining the flow curves and identifying the thermally activated mechanisms that determine the strengthening under given conditions of temperature and strain rate. Regardless of the applied strain rate, higher values of yield stress were noted for 0.25C-1Mn-0.25Si-CrNiMo steel. Microstructures of the examined steels, obtained after cooling the samples from the compression finish temperature, fully correlate with obtained hardness results. Hardness of specimens, obtained from the 0.25C-1Mn-0.25Si-CrNiMo steel grade, cooled in compressed air from the plastic deformation finish temperature (from 900 to 1100 °C), ranges from approx. 517 HV1 to about 431 HV1, while hardness of the 0.75C-1Mn-0.25Si steel samples, produced under the same conditions, ranges from approx. 806 HV1 to about 683 HV1. As part of the work, CCT (Continuous Cooling Transformation) diagrams of the analyzed steels were also calculated, using an original author's program based on artificial neural networks.

**Keywords:** hot deformation, dynamic recovery, dynamic recrystallization, structure.

### INTRODUCTION

Due to the high requirements set by potential recipients of steel products, e.g. the automotive, shipbuilding or mining industries, the proper combination of strength and plastic properties is of particular importance. Nowadays, the required mechanical properties are increasingly often obtained as a result of the interaction of various strengthening mechanisms and the use of the appropriate phase composition of steel [1, 2]. High strength and plastic properties of steels with ferritic-pearlitic microstructure are achieved by grain refinement and precipitation strengthening. Whereas, the mechanical properties of toughened steels depend on the strengthening coming from grain refinement of austenite, precipitation strengthening

and martensitic type phase transitions, as well as from the disintegration of metastable supercooled  $\alpha$  ( $\alpha$  – martensite) solution. Therefore, knowledge of the chemical composition of austenite and control of the grain size of this phase is of great practical meaning. It makes it possible to optimize the chemical composition of steel allowing, at the lowest possible production costs, to obtain the appropriate microstructure, which determines acquiring desired mechanical properties [3]. The assessment of mechanical properties is not equal to the assessment of the suitability of a given material as a construction material. It is also important to have in mind technological properties that can significantly narrow the scope of applications. The effectiveness of individual strengthening mechanisms is determined by chemical constitution of

steel and the parameters of thermo-mechanical treatment [4, 5]. This technology consists in the combination of plastic deformation, using the appropriate advancement of dynamic and static thermally activated processes with controlled cooling of products directly from the temperature of plastic working finish [6-8]. The purpose of the thermo-mechanical treatment is to shape the geometry and required mechanical properties of steel products by controlling structural changes. Knowledge of hot plastic deformation process parameters and their effect on the dislocation structure of steel is the basis for designing modern technologies for manufacturing high-strength steel products [9, 10]. In case of controlled rolling technology, it is important to reduce the charge heating temperature, apply specific rolling reductions in subsequent passes and to accelerate cooling of products after the finish rolling [11]. Simultaneous nucleation of ferrite grains at the  $\gamma$  grain boundaries, deformation bands and other lattice defects as well as recovery and static recrystallization of deformed ferrite, occur during accelerated cooling from the rolling finish temperature [12, 13]. In effect of these procedures, the recrystallization process of deformed austenite is inhibited, and fine ferrite grain, obtained as a result of its transformation, ensures appropriately high strength and plastic properties. It follows that the control of the course of dynamic and static thermally activated processes during hot plastic deformation and cooling, along with the use of phase transformations, create wide possibilities of impacting the microstructure and mechanical properties of steel [14].

Structural changes occurring in hot plastically deformed materials are best illustrated by stress-strain curves ( $\sigma$ - $\varepsilon$ )  $\varepsilon$  – strain,  $\sigma$  – stress, determined most often in high-temperature compression test at a given constant temperature and strain rate [15, 16]. Determined  $\sigma$ - $\varepsilon$  curves characterize the changes in the flow stress, initially at the stage of material strengthening, subsequently – balancing this stage with dynamic recovery or dynamic recrystallization processes – until constant or periodically changing value of the yield stress is obtained at the steady flow stage [17–19].

Alloying elements, both dissolved in solid solution and those that form secondary phase particles, influence the recovery process as well as the dynamic recrystallization process. Alloying elements dissolved in solid solution decrease the recovery rate and, by segregating into

dislocations, make cross slip and the process of their climbing more difficult. This leads to a rapid increase in dislocation density, thereby increasing the driving force of the dynamic recrystallization process and rapid strain hardening [20, 21]. The influence of secondary phase particles on dynamic thermally activated processes depends significantly on their size, shape and distribution in the matrix. If the secondary phase particles are fine and highly dispersed, they stabilize the substructure, hinder the formation of recrystallization fronts and their migration, and inhibit dynamic recovery [22, 23]. However, when secondary phase particles are precipitated at grain boundaries, they can effectively block their migration, and thus inhibit the dynamic recrystallization process without significantly affecting the dynamic recovery. In case of large particles of secondary phases, which interact with dislocations as stress concentrators and, at the same time, constitute privileged sites for heterogeneous formation of recrystallization nuclei, an acceleration of the dynamic recrystallization process is observed [24–26]. For instance, the effect of secondary phase particles on the shape of  $\sigma$ - $\varepsilon$  curves of C-Mn-Si structural steel, with low concentration of alloying elements and microadditions, plastically deformed at the temperature of 900 °C, was studied in [27]. At the temperature of 900 °C, niobium introduced into this steel is completely bound in dispersive NbC carbides, vanadium – partially bound in VC carbides and partially dissolved in solid solution, while Mo – is completely dissolved in solid solution. The results presented in this paper indicate that the highest strain hardening and inhibition of dynamic recrystallization of austenite are caused by introduction of Mo, Nb and V into the steel, causing a simultaneous increase in the lattice friction stress and decrease in the rate of dynamic recovery of solid solution as well as precipitation hardening of the  $\gamma$  phase by dispersive carbide particles. However, combined interaction of Nb and V without the addition of Mo and Nb individually allows for the dynamic recrystallization process.

The aim of this work is to investigate the influence of chemical composition and plastic strain parameters on the yield stress, strengthening mechanisms, microstructure and hardness of low-alloy structural steels.

## MATERIALS AND METHODS

The tests were conducted on structural steels from industrial melts. Technological operations included the industrial process of controlled rolling of steel sheets with the chemical composition given in Table 1. Produced billets, with dimensions of 350 × 385 mm, were the feedstock to the continuous rolling mill of slabs. After hot rolling, slabs measuring 200 × 220 × 5300 mm were used as a stock for controlled sheet rolling process. The feedstock heating temperature was equal 1150 °C, and the rolling finish temperature was equal 850 °C. Samples for testing were cut from produced 20 mm thick sheets.

Examined steels are characterized by different carbon contents (0.25% and 0.75%) and similar concentration of Mn and Si. Microaddition of Ti in a concentration of 0.027% was introduced to the 0.25C-1Mn-0.25Si-CrNiMo steel. This steel can be successfully used for forgings of gears, shafts, pins and other components of gearboxes that carry heavy loads, as well as structural elements operating in difficult climatic conditions. Whereas the chemical composition of 0.75C-1Mn-0.25Si steel was designed for high resistance to abrasive and fatigue wear.

The CCT diagrams of supercooled austenite phase transformation for tested steels were determined in the first place. They were calculated based on the chemical composition of steel and austenitizing temperature with the use of author’s neural model. Artificial neural networks and a data set, prepared on the basis of 550 CCT diagrams published in the literature references, were taken into consideration for the modelling. The neural model was implemented in the author’s computer program [28, 29] for the calculation and graphical presentation of the results.

The axisymmetric hot compression tests were performed in the Gleeble 3800 simulator, equipped with a measuring unit installed in the Hydrowedge system, which allows for accurate

realization of the programmed tests [30]. During the compression test, sample temperature, force on the sample and tool displacement were recorded. The value of the force and tool displacement was the basis for calculating the instantaneous yield stress and strain. Cylindrical samples with 10 mm in diameter and 12 mm in length were used for the purpose of the research. High temperature compression tests were carried out using:

- the continuous compression method to determine the plasticity characteristics of the tested steels in the  $\sigma$ - $\epsilon$  system, depending on the temperature and deformation rate,
- the sequential (four-stage) compression method, physically simulating the rolling process to determine the effect of multiple and most often additive deformation on the shape of flow curves, strengthening mechanisms and microstructure of studied steels.

In order to determine the  $\sigma$ - $\epsilon$  curves of austenite of the examined structural steels, continuous compression tests were performed, which included:

- resistance heating of samples to austenitizing temperature, at a rate of 3 °C/s,
- austenitizing the specimens at the temperature of 1150 °C for 30 s,
- cooling the samples to the set deformation temperature, at a rate of 5 °C/s,
- compression of samples to the actual strain  $\varphi = 0.69$  in the temperature range of 900 °C ÷ 1100 °C, using a strain rate of 0.3 s<sup>-1</sup> and 3 s<sup>-1</sup>,
- cooling of samples from the plastic deformation finish temperature in compressed air, at a rate of approximately 20 °C/s.

The second type of research, using Gleeble 3800 thermo-mechanical simulator, consisted in four-stage hot compression of axisymmetric samples – simulating rolling passes. Detailed test program is presented in Table 2. Heating and cooling rates as well as holding time

**Table 1.** Chemical composition of investigation steels, wt.%

0.25C-1Mn-0.25Si-CrNiMo							
C	Mn	Si	Cr	Ni	Mo	Cu	Ti
0.25	0.94	0.24	0.44	0.63	0.36	0.16	0.027
0.75C-1Mn-0.25Si							
C	Mn	Si	Cr	Ni	Mo	Cu	Ti
0.75	0.98	0.23	0.07	0.09	–	0.24	–

**Table 2.** Parameters of four-stage sample compression

Heating					
Soaking temperature, °C		Heating rate, °C/s		Soaking time, s	
1150		3		30	
Deformation conditions					
No.	Deformation temperature, °C	$\epsilon$	$\dot{\epsilon}$ , s <sup>-1</sup>	Cooling rate to a successive deformation step, °C/s	Time between successive deformation steps, s
1	1000	0.3	0.3 and 3	5.00	10
2	950	0.2	0.3 and 3	10.00	5
3	900	0.2	0.3 and 3	16.66	3
4	850	0.2	0.3 and 3	–	–

at the austenitizing temperature were assumed similarly as in case of continuous compression tests. After austenitizing at the temperature of 1150 °C, specimens were plastically deformed through four-stage compression in the temperature range from 1000 to 850 °C. Similarly to the continuous compression tests, the strain rates of 0.3 s<sup>-1</sup> and 3 s<sup>-1</sup> were applied.

Metallographic specimens were prepared in order to investigate microstructure of steel in as-delivered condition and in plastically deformed state. First, the specimens were ground on abrasive papers with granulation of 400 to 1200 with successive mechanical polishing on polishing wheels dampened with diamond slurry. Metallographic sections of plastically deformed samples were made in a plane consistent with the sample axis, at a distance of 1/3 of the radius from the centre. In order to reveal microstructure, the samples were etched in nital for 5 seconds. Metallographic observations of specimens were performed in Zeiss Axio Observer Z1m light microscope, at magnifications ranging from 50x to 1000x.

The analysis of morphological details of microstructure components and the identification of the chemical composition of revealed non-metallic inclusions were performed in Zeiss Supra scanning electron microscope, using magnification from 1000x to 20000x.

Hardness measurements of the examined steels were carried out on samples in the as-delivered condition, after continuous compression tests and after four-stage plastic deformation. The tests were conducted on FT-ARS 9000 type Vickers hardness tester, applying 9.807 N load. Three measurements were performed for each of the variants.

## RESULTS

### CCT diagrams calculation results

The CCT diagrams of studied steels, determined using artificial neural networks, are presented in Figure 1. Conducted research revealed that 0.25C-1Mn-0.25Si-CrNiMo steel is characterized by  $A_{c3} = 820$  °C,  $A_{c1} = 726$  °C,  $B_s = 579$  °C and  $M_s = 382$  °C, while 0.75C-1Mn-0.25Si steel:  $A_{c3} = 752$  °C,  $A_{c1} = 716$  °C and relatively low  $M_s$  temperature of 234 °C,  $A_{c1}$  – eutectoid transformation temperature during heating,  $A_{c3}$  – finish temperature of the  $\alpha \rightarrow \gamma$  transformation during heating,  $\alpha$  – ferrite;  $\gamma$  – austenite,  $B_s$  – bainitic transformation start temperature,  $M_s$  – martensitic transformation start temperature. What is worth noting is the bainitic and ferritic transformation bay, located close to the temperature axis in case of 0.25C-1Mn-0.25Si-CrNiMo steel, while in case of 0.75C-1Mn-0.25Si steel – pearlitic transformation bay.

### Plastometric tests results

Examination of the hot plastic deformation process of 0.25C-1Mn-0.25Si-CrNiMo steel and 0.75C-1Mn-0.25Si steel, performed in the temperature range from 900 °C to 1100 °C, at the rates of 0.3 s<sup>-1</sup> and 3 s<sup>-1</sup>, allowed determining the influence of compression parameters on the course of the work-hardening curves (Figure 2 and Figure 3). The curves presented in these figures indicate that plastic strain of the investigated steels begins when the yield stress reaches the value of the thermal yield stress. The value of this stress increases with the increase of the strain rate and decrease of the testing temperature. The value of yield stress increases as a result of the increase in density of dislocations in the material

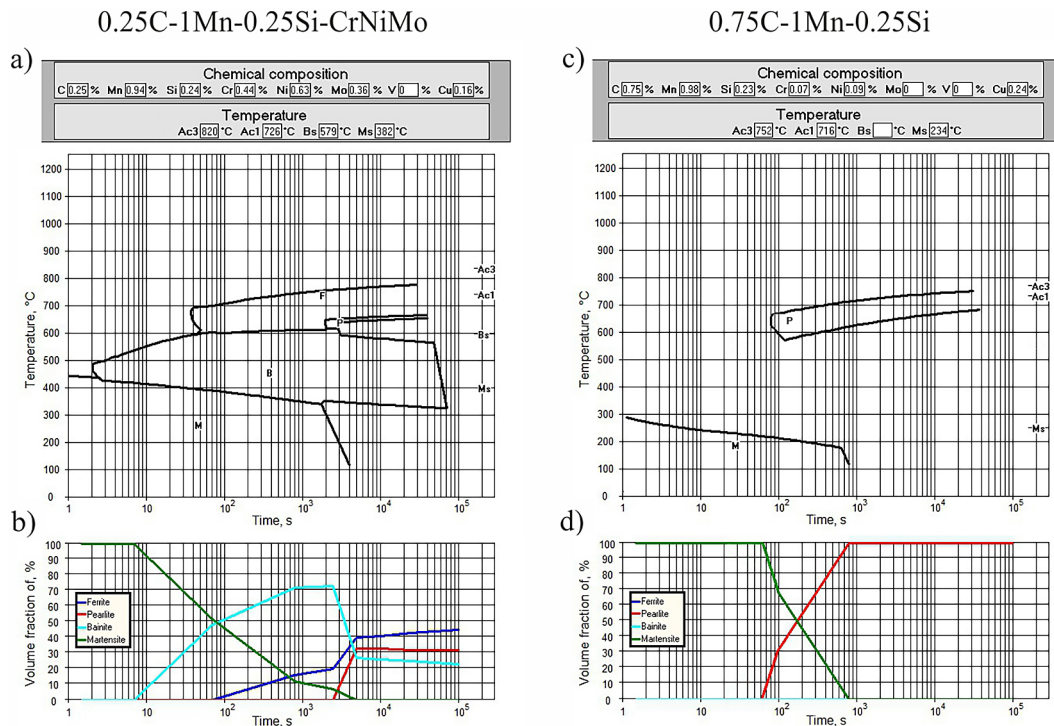


**Figure 1.** Determined CCT diagrams (a, c) and changes in the portion of individual phases as a function of time (b, d) of the examined steel

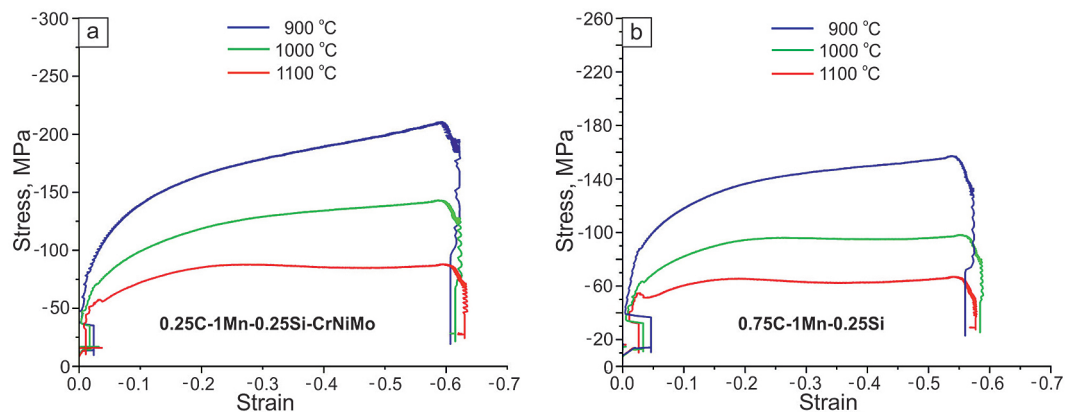


**Figure 2.** Influence of plastic deformation temperature on the shape of  $\sigma$ - $\epsilon$  curves for 0.25C-1Mn-0.25Si-CrNiMo steel (a) and 0.75C-1Mn-0.25Si steel (b), austenitized at the temperature of 1150 °C; strain rate 0.3 s<sup>-1</sup>

microstructure, which results in material strengthening. In case of 0.25C-1Mn-0.25Si-CrNiMo steel, plastically deformed at the rate of 0.3 s<sup>-1</sup> (Figure 2a), in the initial stage of compression, substantial increase of yield stress, as a result of increasing density of dislocations generated in this process, can be observed on work-hardening curves in the range of strain hardening  $\epsilon < 0.025$ . The 0.25C-1Mn-0.25Si-CrNiMo steel samples, compressed at the temperature of 900 °C and 1000 °C, reveal continuous increase in yield

stresses up to the set strain value (Figure 2a – blue and green curve). This means that in case of the 0.25C-1Mn-0.25Si-CrNiMo steel samples, compressed at the temperature of 900 and 1000 °C, at the rate of 0.3 s<sup>-1</sup>, the mechanism controlling the course of plastic deformation is dynamic recovery. Maximum yield stress of the sample, deformed at the temperature of 900 and 1000 °C, is equal 212 MPa and 138 MPa, respectively. Slightly different course is shown by work-hardening curve of the 0.25C-1Mn-0.25Si-CrNiMo

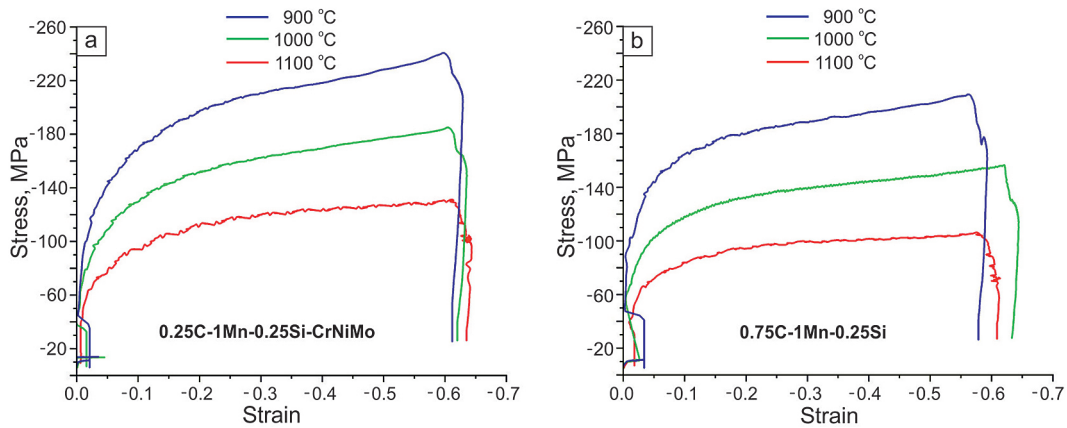


**Figure 3.** Influence of plastic deformation temperature on the shape of  $\sigma$ - $\epsilon$  curves for 0.25C-1Mn-0.25Si-CrNiMo steel (a) and 0.75C-1Mn-0.25Si steel (b), austenitized at the temperature of 1150 °C; strain rate 3 s<sup>-1</sup>

steel, obtained during compression at the temperature of 1100 °C (Figure 2a – red curve). In this case, after reaching the stress corresponding to the thermal yield stress, a small increase in stress occurs until the maximum value of the yield stress is reached ( $\sigma_{\max} = 89$  MPa)  $\sigma_{\max}$  – maximum value of stress. This indicates that thermally activated processes, causing partial softening of emitted dislocations, occur along with formation of new dislocations during the plastic strain. For the strain  $\epsilon_{\max} < \epsilon < \epsilon = 0.6$ , the flow curve is characterized by mild decrease in yield stresses to the equilibrium state value between the hardening process and its decrease due to the thermally activated processes,  $\epsilon_{\max}$  – strain corresponding to the maximum value of the yield stress. This means that in case of 0.25C-1Mn-0.25Si-CrNiMo steel grade, compressed at the temperature of 1100 °C, plastic deformation process is controlled by the course of dynamic recrystallization.

Work-hardening curves for the 0.75C-1Mn-0.25Si steel grade (Figure 2b) reveal lower values of yield stresses compared to 0.25C-1Mn-0.25Si-CrNiMo steel, plastically deformed under the same conditions. This is the result of plastic strain of the examined steels, diversified in terms of chemical composition and primary austenite grain size, after austenitizing at the temperature of 1150 °C. Higher values of yield stress in plastically deformed 0.25C-1Mn-0.25Si-CrNiMo steel are the result of more fine-grained microstructure of austenite, resulting from the presence of precipitations that contain microaddition of Ti, effectively inhibiting the growth of  $\gamma$  phase grains.

The data presented in Figure 2b shows that continuous increase in stress with increasing strain was recorded only in case of the sample compressed at the temperature of 900 °C. This indicates that dynamic recovery is the only mechanism controlling the plastic strain process under these conditions. In case of samples compressed at the temperature of 1000 °C and 1100 °C, a very mild decrease in stresses occurs after the initial increase to the value of  $\epsilon_{\max}$  (0.25 and 0.17, respectively) – corresponding to the maximum values of yield stress  $\sigma_{\max}$  (95 MPa and 65 MPa). This means that for small values of  $\epsilon$  ( $\epsilon < 0.25$  and  $\epsilon < 0.17$ ) plastic deformation process, performed at the temperature of 1000 °C and 1100 °C, is controlled by the dynamic recovery process, whereas for higher values of  $\epsilon$  – by the dynamic recrystallization process.

As expected, the increase in plastic strain rate to 3 s<sup>-1</sup> resulted in increase in the value of the maximum yield stress (Figure 3), regardless of the steel tested. In case of 0.25C-1Mn-0.25Si-CrNiMo steel, continuous increase in yield stress was recorded over the entire strain range, independently from testing temperature (Figure 3a). This means that hot plastic deformation process of 0.25C-1Mn-0.25Si-CrNiMo steel at the rate of 3 s<sup>-1</sup> is controlled by the dynamic recovery, with the maximum values of yield stresses equal approx. 240 MPa, approx. 169 MPa and about 130 MPa, for the temperature of 900 °C, 1000 °C and 1100 °C, respectively.

Lower values of yield stress were demonstrated by 0.75C-1Mn-0.25Si steel (Figure 3b). Similarly to 0.25C-1Mn-0.25Si-CrNiMo steel,

there is a significant increase in stress due to increasing dislocation density in the initial compression phase. In the subsequent compression phase, with increasing strain – regardless of the testing temperature – there is a continuous increase in yield stresses to the assumed strain value. Maximum values of yield stress  $\sigma_{max}$ , at the temperature of 900 °C, 1000 °C and 1100 °C, are approximately equal 210 MPa, approx. 158 MPa and about 105 MPa, respectively. The course of hardening curves of the 0.75C-1Mn-0.25Si steel grade indicates that the mechanism controlling the course of hot plastic deformation process is dynamic recovery.

The result of the four-stage plastic deformation of axisymmetric samples in the temperature range from 1000 °C to 850 °C, at the rate of 0.3s<sup>-1</sup> and 3 s<sup>-1</sup>, are the curves presented in Figure 4. The process that controls strain hardening over the entire temperature range, regardless of the applied strain rate, is dynamic recovery. Similarly as in case of continuous compression tests of samples, higher values of yield stress were noted for 0.25C-1Mn-0.25Si-CrNiMo steel. The differences in maximum yield stress values for studied steels are equal approximately 26 MPa, approx. 30 MPa, approx. 40 MPa and about 60 MPa, for the first, second, third and fourth stage of deformation. In case of four-stage compression test of 0.25C-1Mn-0.25Si-CrNiMo steel grade, at the rate of 0.3 s<sup>-1</sup> (Figure 4a), initially there is a gradual increase in yield stress value from approx. 125 MPa to 145 MPa for plastic deformation temperature of 950°C. For the last deformation temperature of 850 °C, more rapid increase in the yield stress occurs, related to both

lower temperature and short interval between the third and fourth deformation.

As expected, applying higher rate  $\dot{\epsilon} = 3$  ( $\dot{\epsilon} = 3 \text{ s}^{-1}$ )  $\dot{\epsilon}$  – strain rate, in the four-stage deformation test results in higher yield stress values over the entire temperature range (Figure 4b). Similarly to the four-stage compression test at the rate of 0.3 s<sup>-1</sup>, higher values of the maximum yield stress are demonstrated by 0.25C-1Mn-0.25Si-CrNiMo steel. In the examined temperature range, the following stress values were noted: approx. 152 MPa, approx. 175 MPa, approx. 220 MPa and about 270 MPa, for the temperature of 1000 °C, 950 °C, 900 °C and 850 °C, respectively. Whereas in case of 0.75C-1Mn-0.25Si steel, the maximum yield stress for the above-mentioned temperatures equals as follows: approx. 125 MPa, approx. 146 MPa, approx. 178 MPa and about 237 MPa, respectively.

### Metallographic examination results

The results of microstructure observations of 0.25C-1Mn-0.25Si-CrNiMo and 0.75C-1Mn-0.25Si steel in the as-delivered condition and after continuous compression of samples and their subsequent cooling in compressed air are presented in Figures 5–7. The 0.25C-1Mn-0.25Si-CrNiMo steel grade, containing 0.25% C, in the as-delivered condition – after cooling in open air from the rolling finish temperature, is characterized by fine-grained ferritic-pearlitic microstructure (Figure 5a, b). Whereas 0.75C-1Mn-0.25Si steel grade (0.75% C), in the as-delivered condition, demonstrates pearlitic microstructure (Figure 5c, d). Microstructure of 0.25C-1Mn-0.25Si-CrNiMo and 0.75C-1Mn-0.25Si steel, obtained after

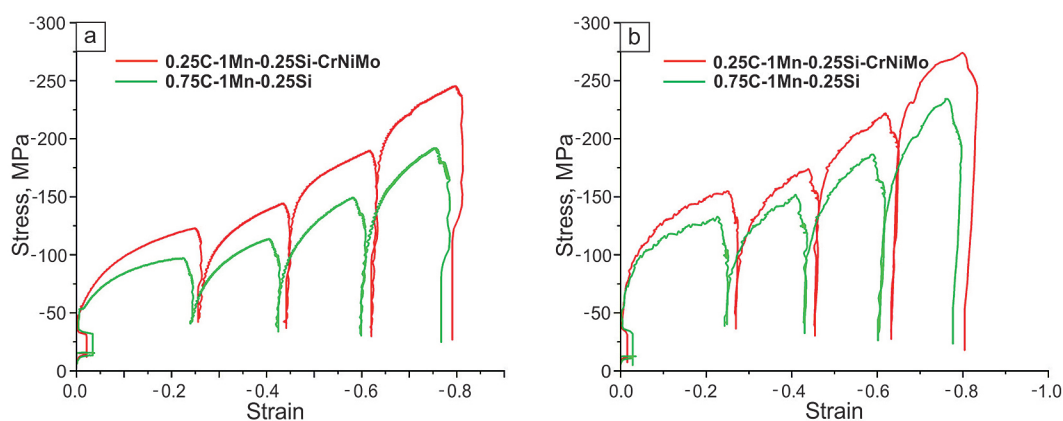


**Figure 4.** Influence of chemical composition and deformation rate on a shape of  $\sigma$ - $\epsilon$  investigated steels austenitizing in temperature of 1150 °C; strain rate 0.3 s<sup>-1</sup> (a) and 3 s<sup>-1</sup> (b)

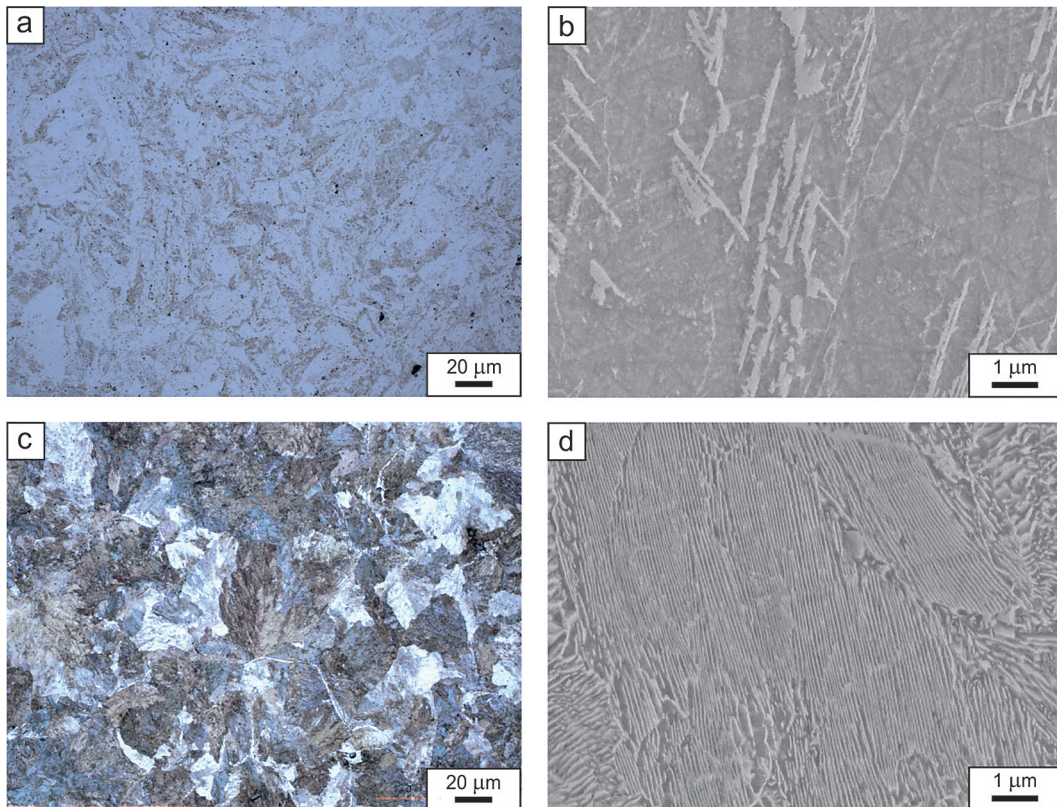


**Figure 5.** Microstructures of tested steels in the as-delivered condition: a, b – ferritic-pearlitic microstructure of 0.25C-1Mn-0.25Si-CrNiMo steel, c, d – pearlitic microstructure of 0.75C-1Mn-0.25Si steel

cooling in compressed air immediately after finishing the compression at the rate of  $0.3 \text{ s}^{-1}$ , in the temperature range from  $900 \text{ }^{\circ}\text{C}$  to  $1100 \text{ }^{\circ}\text{C}$ , are presented in Figure 6. The 0.25C-1Mn-0.25Si-CrNiMo steel samples, produced under these conditions, obtain bainitic-martensitic-ferritic microstructure (Figure 6a-c). It was pointed out that the specimens cooled from the plastic deformation finish temperature of  $900 \text{ }^{\circ}\text{C}$  are characterized by fine-grained microstructure (Figure 6a). An increase in the plastic strain temperature to  $1100 \text{ }^{\circ}\text{C}$  results in formation of more coarse-grained microstructure (Figure 6c).

Figure 6d-f show microstructures of the 0.75C-1Mn-0.25Si steel samples compressed at the rate of  $0.3 \text{ s}^{-1}$ , in the same temperature range as the 0.25C-1Mn-0.25Si-CrNiMo steel samples. The 0.75C-1Mn-0.25Si steel grade samples show martensitic microstructure. Similar microstructure was demonstrated for samples of the tested steels compressed at the rate of  $3 \text{ s}^{-1}$ . The microstructure of 0.25C-1Mn-0.25Si-CrNiMo steel is bainitic-martensitic-ferritic (Figure 7a-c), and the 0.75C-1Mn-0.25Si – martensitic with a large number of non-metallic inclusions of various sizes and morphology (Figure 7d-f). Performed

analysis of chemical composition of revealed non-metallic inclusions indicated that, in majority of cases, they were MnS type sulphides and  $\text{Al}_2\text{O}_3$  type oxides (Figure 8).

The increase in strain rate resulted in formation of more fine-grained microstructure, especially in case of 0.25C-1Mn-0.25Si-CrNiMo steel grade. Plastic deformation of studied steels in the process of four-stage compression of samples, in the temperature range from  $1000 \text{ }^{\circ}\text{C}$  to  $850 \text{ }^{\circ}\text{C}$  and their subsequent cooling in compressed air, resulted in formation of more fine-grained microstructures in comparison with those obtained after continuous compression, especially in case of 0.25C-1Mn-0.25Si-CrNiMo steel. As an example, Figure 9 shows microstructure of 0.25C-1Mn-0.25Si-CrNiMo steel, obtained after four-stage compression, at the rate of  $0.3 \text{ s}^{-1}$  and  $3 \text{ s}^{-1}$ .

### Hardness measurement results

Hardness measurements of samples in as-delivered condition showed that 0.25C-1Mn-0.25Si-CrNiMo steel is characterized by average hardness of 274 HV1, while the

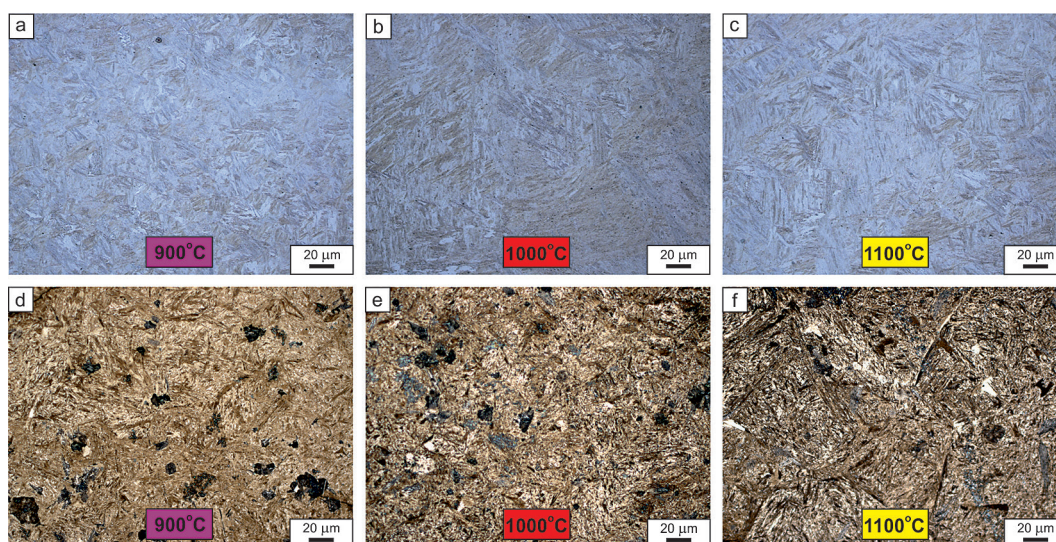


**Figure 6.** Microstructures obtained after cooling the samples in compressed air from the plastic deformation finish temperature: a, b, c – 0.25C-1Mn-0.25Si-CrNiMo steel, d, e, f – 0.75C-1Mn-0.25Si steel; strain rate  $0.3 \text{ s}^{-1}$

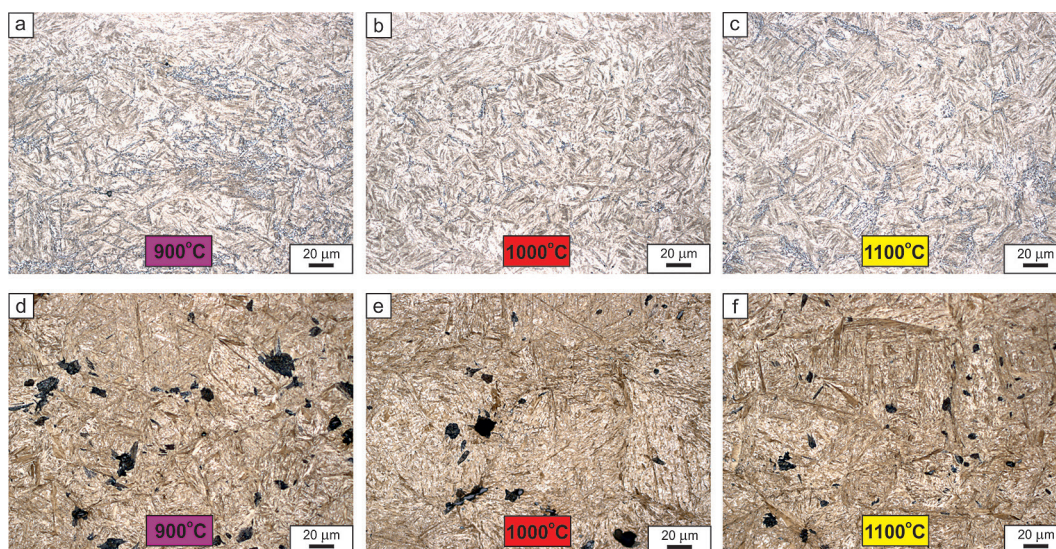


**Figure 7.** Microstructures obtained after cooling the samples in compressed air from the plastic deformation finish temperature: a, b, c – 0.25C-1Mn-0.25Si-CrNiMo steel, d, e, f – 0.75C-1Mn-0.25Si steel; strain rate  $3 \text{ s}^{-1}$

average hardness observed for the 0.75C-1Mn-0.25Si steel is equal 401 HV1. Obtained hardness measurement results fully correspond with the microstructure revealed in this state (Figure 5). Hardness tests were also conducted on samples after continuous compression in the temperature range from 900 °C to 1100 °C, then cooled directly from the plastic deformation finish temperature in compressed air. Detailed results of hardness measurements of samples, compressed in the above-mentioned temperature range, at the rate of  $0.3 \text{ s}^{-1}$  and  $3 \text{ s}^{-1}$ , are presented in Table 3. The data shown in this table indicate that,

regardless of the applied deformation rate, the 0.75C-1Mn-0.25Si steel samples exhibit higher hardness than 0.25C-1Mn-0.25Si-CrNiMo steel in the entire test temperature range. This is the result of varied microstructure of the examined steels. The 0.75C-1Mn-0.25Si steel, after cooling in compressed air, reveals martensitic microstructure, and the 0.25C-1Mn-0.25Si-CrNiMo steel – bainitic-martensitic-ferritic microstructure. The average hardness of 0.75C-1Mn-0.25Si steel samples, after continuous compression at the temperature of 900 °C, 1000 °C and 1100 °C and subsequent cooling in compressed air to

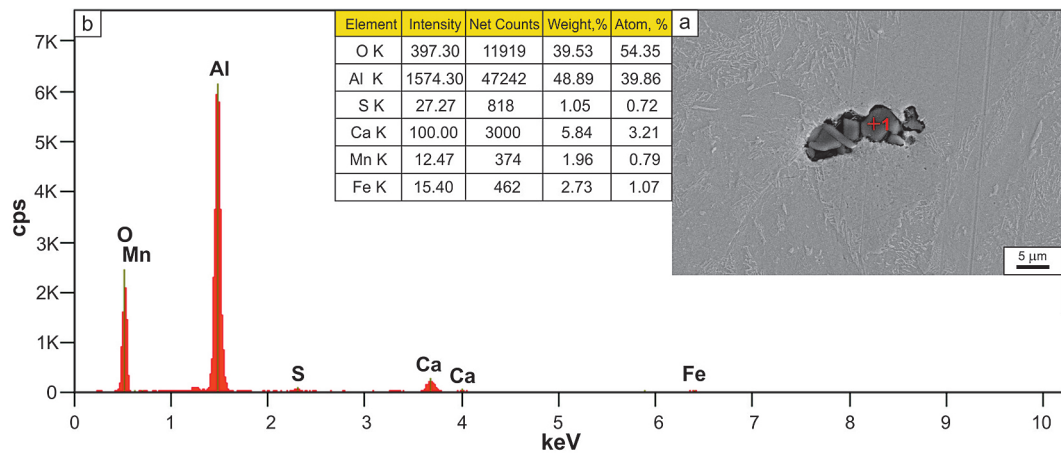


**Figure 8.** Non-metallic inclusion of the  $Al_2O_3$  type in 0.75C-1Mn-0.25Si steel: a – a view of inclusion; b – spectrometric spectrum of non-metallic inclusion; strain temperature of 1100 °C; strain rate  $3\ s^{-1}$

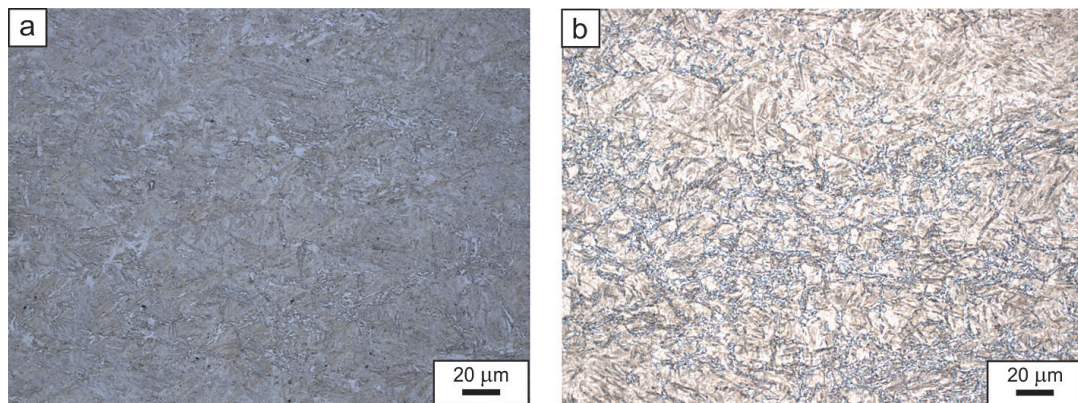


**Figure 9.** Microstructure of 0.25C-1Mn-0.25Si-CrNiMo steel obtained after four-stage compression of samples at the rate of  $0.3\ s^{-1}$  (a) and  $3\ s^{-1}$  (b) and cooling in compressed air

**Table 3.** The results of hardness measurements of the tested steels after the continuous compression test

Steel designation	Hardness, HV1					
	$\dot{\epsilon} = 3\ s^{-1}$			$\dot{\epsilon} = 3\ s^{-1}$		
	900 °C	1000 °C	1100 °C	900 °C	1000 °C	1100 °C
0.25C-1Mn-0.25Si-CrNiMo	424	460	499	429	512	529
	456	403	497	535	506	534
	414	520	470	489	534	479
	<b>431</b>	<b>461</b>	<b>489</b>	<b>484</b>	<b>517</b>	<b>514</b>
0.75C-1Mn-0.25Si	689	622	668	817	823	836
	764	691	711	753	790	759
	684	739	695	729	805	781
	<b>712</b>	<b>683</b>	<b>691</b>	<b>766</b>	<b>806</b>	<b>792</b>

ambient temperature, is equal 712 HV1, 683 HV1 and 691 HV1, respectively – for the strain rate of  $0.3\ s^{-1}$  and 766 HV1, 806 HV1 and 792 HV1 – for the strain rate of  $3\ s^{-1}$ . Whereas hardness of the 0.25C-1Mn-0.25Si-CrNiMo steel samples,

produced under the same conditions, varies from 431 HV1 to 489 HV1 – for the strain rate of  $0.3\ s^{-1}$  and from 484 HV1 to 514 HV1 – for a strain rate of  $3\ s^{-1}$ . This indicates that hardness of examined steel samples varies only slightly

within the applied temperature range. Hardness was also measured on samples after four-stage plastic deformation in the temperature range from 1000 °C to 850 °C and subsequent cooling in the same way as for samples subjected to continuous compression. The average hardness of the 0.75C-1Mn-0.25Si steel samples, obtained under these conditions, is equal 810 HV1 and 794 HV1 – for the strain rate of 0.3 s<sup>-1</sup> and 3 s<sup>-1</sup>, respectively, and the 0.25C-1Mn-0.25Si-CrNiMo steel samples – 482 HV1 and 442 HV1.

## DISCUSSION

The CCT diagrams shown in Figure 1 were calculated based on chemical composition of the steel and given austenitizing conditions. Performed calculations allowed determining characteristic temperatures ( $A_{c3}$ ,  $A_{c1}$ ,  $B_s$  and  $M_s$ ) and temperature-time areas of individual phase transformations of supercooled austenite. The data presented in Figure 1a reveal that 0.25C-1Mn-0.25Si-CrNiMo steel exhibits a very wide range of occurrence of the bainitic transformation bay, with the temperature  $B_s = 579$  °C. The initiation of bainitic transformation begins after only 2 s, and ferritic transformation after 40 s. The data presented in Figure 1a indicate that 0.25C-1Mn-0.25Si-CrNiMo steel, cooled at high rate, will demonstrate martensitic-bainitic microstructure; however this steel will exhibit bainitic-martensitic-ferritic microstructure in a very wide range of cooling rates. What is worth noting when analyzing the CCT diagram of 0.75C-1Mn-0.25Si steel is low temperature  $M_s = 234$  °C, the absence of bainitic transformation and the pearlitic transformation bay located relatively close to the temperature axis (Figure 1c). Obtained calculation results were used as a reference point for determining the conditions of plastometric tests.

Studies of high-temperature plastic deformation process of 0.25C-1Mn-0.25Si-CrNiMo and 0.75C-1Mn-0.25Si steel allowed to determine the influence of temperature (900 ÷ 1100 °C) and strain rate ( $\dot{\epsilon} = 0.3$  s<sup>-1</sup> and  $\dot{\epsilon} = 3$  s<sup>-1</sup>) on the hardening phenomenon, recovery and recrystallization processes of deformed austenite, based on the analysis of the course of the  $\sigma$ - $\epsilon$  flow curves, as well as the characteristic values of the recorded stresses and strains. The 0.25C-1Mn-0.25Si-CrNiMo steel with microaddition of Ti at a concentration of 0.027%, deformed in a high-temperature

compression test to  $\phi = 0.69$ , reveals a different course of flow curves, depending mainly on the temperature and deformation rate. After austenitizing at the temperature of 1150 °C and deformation at the temperature of 1100 °C, at the rate of 0.3 s<sup>-1</sup>, recorded curve is characterized by indistinct flow stress maximum and limited range of steady-state stresses, conditioned by the course of dynamic recrystallization. At lower deformation temperatures (900 °C and 1000 °C), the dynamic recrystallization process is not revealed (Figure 2a). The actual strain in realized compression tests is too low to initiate the dynamic recrystallization process in the tested steel. Under these deformation conditions, the decisive process that completely eliminates the effects of strain hardening is dynamic recovery.

Increasing the strain rate of the 0.25C-1Mn-0.25Si-CrNiMo steel to 3 s<sup>-1</sup> resulted in continuous increase in the yield stresses visible on the  $\sigma$ - $\epsilon$  curves over the entire strain range, regardless of the applied test temperature (Figure 3a). This means that for the above-mentioned parameters dynamic recovery is the only mechanism controlling the course of plastic strain process. Very similar results, i.e. the shape of the  $\sigma$ - $\epsilon$  curves and the values of yield stress, were obtained by the authors of [31], in which the hot formability of steel, containing 0.16% C, 1.48% Mn, 0.29% Si and 0.004% Ti, was investigated. Samples of this steel were compressed at the temperature of 900 °C, 1000 °C, 1100 °C and 1250 °C, at the rate of  $\dot{\epsilon} = 1$  s<sup>-1</sup> and  $\dot{\epsilon} = 3.6$  s<sup>-1</sup>. Similarly to the analyzed 0.25C-1Mn-0.25Si-CrNiMo steel, the dynamic recrystallization process occurred only at the temperature of 1100 °C and above, and only for low strain rates. This is consistent with the results obtained in [32, 33], where the inhibiting effect of Ti microaddition on the dynamic recrystallization process, also with significant effect of Mo addition, was demonstrated. Dispersive Ti carbide particles, precipitating in plastically deformed austenite at dislocations, grain boundaries and other lattice defects, inhibit dynamic recrystallization and, at the same time, increase the lattice friction stress and reduce the rate of dynamic recovery of solid solution as well as precipitation hardening of austenite [34].

Hot formability tests of 0.75C-1Mn-0.25Si steel have shown that, regardless of the test temperature and deformation rate, this steel is characterized by lower yield stress values compared to 0.25C-1Mn-0.25Si-CrNiMo steel.

The reason for higher values of yield stress of 0.25C-1Mn-0.25Si-CrNiMo steel is its more fine-grained microstructure, resulting from the presence of dispersive particles containing Ti, which effectively inhibit the growth of austenite grains. The  $\sigma$ - $\varepsilon$  curve, recorded during compression of the 0.75C-1Mn-0.25Si steel sample at the temperature of 900 °C, at the rate of 0.3 s<sup>-1</sup>, reveals continuous increase in yield stress (Figure 2b). Under these conditions, the process controlling the course of plastic deformation is dynamic recovery. At higher strain temperatures (1000 °C and 1100 °C), the  $\sigma$ - $\varepsilon$  curves demonstrate slight decrease in the flow stress versus strain after reaching  $\sigma_{\max}$  due to stress relaxation, resulting from thermally activated processes, in particular dynamic recrystallization. Increasing the strain rate of 0.75C-1Mn-0.25Si steel to 3 s<sup>-1</sup> resulted in increase in yield stresses in the entire strain range. The course of  $\sigma$ - $\varepsilon$  curves, recorded for this steel, is typical for the dynamic recovery process (Figure 3b). The plasticity characteristics for 0.75C-1Mn-0.25Si steel are very similar to those obtained in [35], where plasticity characteristics were determined for pearlitic steel, containing 0.67% C, 1.02% Mn and 0.25% Si in the temperature range of 800 ÷ 1000 °C.

The  $\sigma$ - $\varepsilon$  curves obtained after four-stage compression of samples in the temperature range from 1000 °C to 850 °C indicate that, in the entire strain range, the only mechanism eliminating the effects of hardening is dynamic recovery. The values of yield stress increase significantly with decreasing strain temperature, and they are similar to the stress values obtained in continuous compression test – for the temperatures (900 °C and 1000 °C). Moreover, these tests showed that higher yield stress values were observed in the 0.25C-1Mn-0.25Si-CrNiMo steel over the entire test temperature range, regardless of the applied strain rate (Figure 4).

Metallographic observations of analyzed steels in the as-delivered condition revealed that they are characterized by microstructures consistent with the phase equilibrium system, i.e. 0.25C-1Mn-0.25Si-CrNiMo steel – ferritic-pearlitic microstructure (Figure 5a, b), and 0.75C-1Mn-0.25Si steel – pearlitic microstructure (Figure 5c, d). Microstructures of the 0.25C-1Mn-0.25Si-CrNiMo steel samples, cooled in compressed air directly from the plastic deformation finish temperature (900 °C ÷ 1100 °C), are presented in Figure 6a-c and

Figure 7a-c. The 0.25C-1Mn-0.25Si-CrNiMo steel samples, produced under these conditions, demonstrate bainitic-martensitic-ferritic microstructure. Revealed microstructures fully correlate with the CCT diagram determined for this steel (Figure 1a). Considering that plastic deformation of austenite prior to transformation causes significant acceleration of ferritic transformation [36–39], the presence of ferrite in microstructure of 0.25C-1Mn-0.25Si-CrNiMo steel samples, cooled in compressed air from plastic deformation finish temperature, is fully justified. The 0.75C-1Mn-0.25Si steel samples, produced under the same conditions, have martensitic microstructure with a large number of non-metallic inclusions (Figure 6d-f and Figure 7d-f). Disclosed inclusions are mainly MnS type sulphides and Al<sub>2</sub>O<sub>3</sub> type oxides (Figure 8), with the length/diameter of these inclusions reaching up to 20 µm. The presence of such inclusions in microstructure may contribute to the occurrence of anisotropy of plastic properties of rolled products, especially sheets and pipes, usually expressed by the ratio of the fracture energy of Charpy V-shaped specimens, transverse and parallel to the rolling direction. Non-metallic inclusions of this type are also often the cause of delamination and lamellar cracks in welded joints of sheets, plastically pre-deformed in the hot state, and the sensitivity of welded joints to cracking in the heat-affected zone [8].

In conclusion, it is necessary to emphasize the practical usefulness of the obtained results. The article presents important information useful for engineers designing steel alloys, especially when it is about selecting the chemical composition, plastic working parameters and predicting the microstructure and mechanical properties of the material. Calculated CCT curves are the basis for the correct design of heat treatment technologies. The determined technological plasticity characteristics are necessary to evaluate the strength and energy parameters of the plastic working process and allow for a comparative assessment of the plasticity of materials from separate melts, depending on the chemical composition, microstructure and production conditions. Moreover, the obtained results of physical simulation of rolling, usually supplemented with the results of numerical simulations, are the basis for designing the rolling scheme using the thermo-mechanical treatment method in semi-industrial lines.

## CONCLUSIONS

Performed research allowed formulating the following conclusions:

1. The CCT curves of the investigated steels, calculated using developed author's computer program, were the basis for determining the conditions of the plastometric tests.
2. Continuous compression of the 0.25C-1Mn-0.25Si-CrNiMo and 0.75C-1Mn-0.25Si steel samples allowed to determine the influence of temperature (900–1100 °C) and strain rate ( $\dot{\epsilon} = 0.3 \text{ s}^{-1}$  and  $\dot{\epsilon} = 3 \text{ s}^{-1}$ ) on the hardening phenomenon, recovery processes and recrystallization of deformed austenite based on the  $\sigma$ - $\epsilon$  curves analysis.
3. Four-stage compression of the examined steel samples in the temperature range from 1000 °C to 850 °C revealed that, in the entire deformation range, the only mechanism eliminating the effects of strain hardening is dynamic recovery.
4. Both, during continuous and four-stage compression tests, higher values of yield stress – regardless of the applied strain rate – were noted for 0.25C-1Mn-0.25Si-CrNiMo steel. This is due to more fine-grained microstructure of austenite compared to 0.75C-1Mn-0.25Si steel, guaranteed by the impact of Ti microaddition.
5. The 0.25C-1Mn-0.25Si-CrNiMo steel samples, cooled in compressed air directly from the plastic deformation finish temperature, reveal bainitic-martensitic-ferritic microstructure, and the 0.75C-1Mn-0.25Si steel samples, produced under the same conditions – martensitic microstructure with considerable number of non-metallic inclusions.
6. Hardness of the 0.25C-1Mn-0.25Si-CrNiMo steel samples, after cooling in compressed air from the temperature of plastic deformation finish (900–1100 °C) changes from 431 HV1 to 517 HV1, while hardness of the 0.75C-1Mn-0.25Si steel specimens – from 683 HV1 to 806 HV1.

## Acknowledgements

Scientific work supported by the Rector's pro-quality grant of the 2<sup>nd</sup> degree. Silesian University of Technology, grant number 10/010/RGJ25/1232.

## REFERENCES

1. Chen W., Gao P., Wang S., Zhao X., Zhao Z. Strengthening mechanisms of Nb and V microalloying high strength hot-stamped steel. *Materials Science and Engineering A* 2020; 797: 140115.
2. Yao Z., Huang Z., Lyu S., Tang F., Zhao B., Ma X. Characterization and strengthening mechanisms of high-strength medium carbon spring steels. *Journal of Materials Research and Technology* 2023; 27: 1395–1405.
3. Long X.Y., Branco R., Macek W., Masoudi Nejad R., Lesiuk G., Zhu S.P., Amaro A.M. Effect of austempering temperature on microstructure and cyclic deformation behaviour of multiphase low-carbon steel. *Archives of Civil and Mechanical Engineering* 2023; 23: 1–17.
4. Wang X., Liu C., Qin Y., Li Y., Yang Z., Long X., Wang M., Zhang F.C. Effect of tempering temperature on microstructure and mechanical properties of nanostructured bainitic steel. *Materials Science and Engineering A* 2022; 832: 142357.
5. Long X.Y., Zhang F.C., Zhang C.Y. Effect of Mn content on low-cycle fatigue behaviors of low-carbon bainitic steel. *Materials Science and Engineering A* 2017; 697: 111–118.
6. Singh P., Mula S., Ghosh S. Grain refinement, strain hardening and fracture in thermomechanically processed ultra-strong microalloyed steel. *Materials Today Communications* 2024; 38: 107582.
7. Reitz A., Grydin O., Schaper M. Influence of thermomechanical processing on the microstructural and mechanical properties of steel 22MnB5. *Materials Science and Engineering A* 2022; 838: 142780.
8. Opiela M., Grajcar A. Microstructure and anisotropy of plastic properties of thermomechanically-processed HSLA-type steel plates. *Metals* 2018; 8(5): 1–15.
9. Lan L., Zhou W., Kong X., Qiu Ch. Hot plastic deformation behavior and its effect on microstructure of low carbon multi-microalloyed steel. *Procedia Engineering* 2017; 207: 651–656.
10. Puchi-Cabrera E.S., Guérin J.D., Barbier D., Dubar M., Lesage J. Plastic deformation of structural steels under hot-working conditions. *Materials Science and Engineering A* 2013; 559: 268–275.
11. Gosh S., Mula S., Malakar A., Somani M., Kömi J. High cycle fatigue performance, crack growth and failure mechanisms of an ultrafine-grained Nb+Ti stabilized, low-C microalloyed steel processed by multiphase controlled rolling and forging. *Materials Science and Engineering A* 2021; 825: 141883.
12. Chen S., Li L., Peng Z., Huo X., Gao J. Strain-induced precipitation in Ti microalloyed steel by two-stage controlled rolling process. *Journal of*

- Materials Research and Technology 2020; 9(6): 15759–15770.
13. Dhua S.K., Sakar P.P. Development of ultrafine grains in C-Mn steel plates through hot-rolling and air-cooling. *Materials Science and Engineering A* 2013; 575: 177–188.
  14. Ali M., Seppälä O., Fabritius T., Kömi J. Microstructure evolution and static recrystallization kinetics in hot-deformed austenite of coarse-grained Mo-free and Mo containing low-carbon CrNiMnB ultrahigh-strength steels. *Materials Today Communications* 2022; 33: 104676.
  15. Opiela M. Thermomechanical treatment of Ti-Nb-V-B micro-alloyed steel forging. *Materiali in Tehnologije* 2014; 48(4): 587–591.
  16. Singh P., Ghosh S., Mula S. Flow stress modeling and microstructural characteristic of a low carbon Nb-V microalloyed steel. *Materials Today Communications* 2022; 30: 103156.
  17. Zhang K., Zhang T., Zhang M., Chen Z., Pan H., Yang G., Cao Y., Li Z., Zhang X. Hot deformation behavior, dynamic recrystallization mechanism and processing maps of Ti-V microalloyed high strength steel. *Journal of Materials Research and Technology* 2023; 25: 4201–4215.
  18. Ebrahimi G.R., Momeni A., Kazemi S., Alinejad H. Flow curves, dynamic recrystallization and precipitation in a medium carbon low alloy steel. *Vacuum* 2017; 142: 135–145.
  19. Dong Ch., Zhao X. Dynamic recrystallization behavior and microstructure evolution of high-strength low-alloy steel during hot deformation. *Journal of Materials Research and Technology* 2023; 25: 6087–6098.
  20. Zhao B., Zhao T., Li G., Lu Q. The kinetics of dynamic recrystallization of low-carbon vanadium-nitride microalloyed steel. *Materials Science and Engineering A* 2014; 604: 117–121.
  21. Lan L., Qiu Ch., Zhao D., Gao X., Du L. Dynamic and static recrystallization behavior of low carbon high niobium microalloyed steel. *Journal of Iron and Steel Research, International* 2011; 18(1): 55–60.
  22. Mishra B., Singh V., Sakar R., Mukhopadhyay A., Gopinath K., Madhu V., Prasad M.J. Dynamic recovery and recrystallization mechanisms in secondary B2 phase and austenite matrix during hot deformation of Fe-Mn-Al-C-(Ni) based austenitic low-density steels. *Materials Science and Engineering A* 2022; 842: 143095.
  23. Sun Z., Shen D., Sun W., Tang B. Influence of stress state and dynamic recrystallization on fracture behavior in hot forming of Cr and Mo alloyed Fe-C-Mn steel. *Engineering Failure Analysis* 2025; 171: 109339.
  24. Zhang T., Li Z., Zhang K., Fu X., Cao Y., Zhang X., Li Z. Comprehensive analysis of Fe-Mn-Al-C lightweight steel: Hot deformation behavior, dynamic recrystallization mechanisms and numerical simulation. *Vacuum* 2025; 234: 114012.
  25. Liu C., Peng Y., Barella S., Mapelli C., Liang S. Characterization of dynamic recrystallization behavior of low carbon steel under flexible rolling process. *Materials Today Communications* 2021; 29: 102777.
  26. Adedi H.R., Hanzaki A., Liu Z., Xin R., Haghdad N., Hodgson P.D. Continuous dynamic recrystallization in low density steel. *Materials & Design* 2017; 114: 55–64.
  27. Akben M.G., Jonas J.J. Influence of multiple microalloy additions on the flow stress and recrystallization behavior of HSLA steels. In: *Proceedings of International Conference on Technology and Applications of HSLA Steels, Philadelphia, USA* 1983: 149–161.
  28. Trzaska J. A new neural networks model for calculating the continuous cooling transformation diagrams. *Archives of Metallurgy and Materials* 2018; 63: 2009–2015.
  29. Trzaska J. Prediction methodology for the anisothermal phase transformation curves of the structural and engineering steels. *Silesian University of Technology Press, Gliwice, Poland* 2017 (in Polish).
  30. Lee R.S., Lin Y.K., Chien T.W. Experimental and theoretical studies on formability of 22MnB5 at elevated temperatures by Gleeble simulator. *Procedia Engineering* 2014; 81: 1682–1688.
  31. Gnapowski S., Opiela M., Kalinowska-Ozgowicz E., Szulzyk-Cieplak J. The effect of hot deformation parameters on the size of dynamically recrystallized austenite grains of HSLA steel. *Advances in Science and Technology. Research Journal* 2020; 14(2): 76–84.
  32. Zhou F., Guo J., Zhao Y., Chu X., Liu L., Zhou Ch., Zhao Z. An improved cellular automaton model of dynamic recrystallization and the constitutive model coupled with dynamic recrystallization kinetics for microalloyed high strength steels. *Journal of Materials Research and Technology* 2024; 33: 10003–10021.
  33. Arribas M., López B., Rodrigues-Ibabe J.M. Additional grain in recrystallization controlled rolling of Ti-microalloyed steels processed by near-net-shape casting technology. *Materials Science and Engineering A* 2008; 485(1-2): 383–394.
  34. He P., Hu H., Wang W., Wang L., Xu G. On the correlation among isothermal transformation, interphase precipitation behaviour and elements partitioning in Ti-Mo microalloyed steel. *Journal of Materials Research and Technology* 2024; 29: 1901–1910.
  35. Kalinowska-Ozgowicz E. Structural and mechanical factors of the strengthening and recrystallization

- of hot plastic deformation of steels with microadditives. *Scientific International Journal of the World Academy of Materials and Manufacturing Engineering* 2013; 20(2):1–246.
36. Grajcar A., Opiela M. Influence of plastic deformation on CCT-diagrams of low-carbon and medium-carbon TRIP-steels. *Journal of Achievements in Materials and Manufacturing Engineering* 2008; 29: 71–78.
37. Yin S., Sun X., Liu Q., Zhang Z. Influence of deformation on transformation of low-carbon and high Nb-containing steel during continuous cooling. *Journal of Iron and Steel Research* 2010; 17: 43–47.
38. Olasoslo M., Uranga P., Rodrigues-Ibabe J.M., López B. Effect of austenite microstructure and cooling rate on transformation characteristic in a low carbon Nb-V microalloyed steel. *Materials Science and Engineering A* 2011; 528: 2559–2569.
39. Eghbali B., Abdollah-Zadeh A. Deformation-induced ferrite transformation in a low carbon Nb-Ti microalloyed steel. *Materials and Design* 2007; 28: 1021–1026.